

Cite this: DOI: 10.1039/xxxxxxxxxx

## Sub-100 nm wrinkling of polydimethylsiloxane by double frontal oxidation‡

Manuela Nania,<sup>a</sup> Fabrizia Foglia,<sup>a</sup> Omar K. Matar,<sup>a</sup> and João T. Cabral<sup>\*a</sup>

Received Date  
Accepted Date

DOI: 10.1039/xxxxxxxxxx

www.rsc.org/journalname

We demonstrate nanoscale wrinkling on polydimethylsiloxane (PDMS) at sub-100 nm length scales via a (double) frontal surface oxidation coupled with a mechanical compression. The kinetics of the glassy skin propagation is resolved by neutron and X-ray reflectivity, and atomic force microscopy, combined with mechanical wrinkling experiments to evaluate the resulting pattern formation. In conventional PDMS surface oxidation, the smallest wrinkling patterns attainable have an intrinsic lower wavelength limit due to the coupling of skin formation and front propagation at fixed strain  $\epsilon_{prestrain}$ , whose maximum is, in turn, set by material failure. However, combining two different oxidative processes, **an ultra-violet ozonolysis followed by air plasma exposure**, we break this limit by fabricating trilayer laminates with excellent interfacial properties and a sequence of moduli and layer thicknesses able to trivially reduce the surface topography to sub-100 nm dimensions. This method provides a powerful, yet simple, non-lithographic approach to extend surface patterning from visible to the deep UV range.

### 1 Introduction

Nano-structured surfaces exhibit unique optical, physical, mechanical and electronic properties<sup>1,2</sup>. Conventional nanofabrication techniques, including electron and focused ion beam lithography (EBL, FIB)<sup>3–6</sup> nanoimprint lithography<sup>7–9</sup> and photolithography<sup>10</sup>, are generally low throughput and costly for large area patterning<sup>11</sup>. Bottom-up methods<sup>12</sup>, including block-copolymer self-assembly<sup>13</sup> or a range of surface instabilities<sup>14</sup> provide thus attractive alternatives. Mechanically-induced wrinkling of bilayers<sup>15–17</sup> has been extensively used for a plethora of applications in surface science, optics and photonics, biology and microfabrication<sup>18–20</sup>. These range from the fabrication of super-hydrophobic or directional wetting surfaces<sup>21</sup>, to tuneable lasers<sup>22</sup> and cell sorting<sup>23</sup> and proliferation<sup>24</sup>. Highly-ordered patterns can be formed by compression of bi- or multi-layer structures with mismatched moduli, which can be readily induced mechanically, thermally or due to a volume change (e.g. film drying), in both uni- and multi-axial geometries. Whilst several film fabrication methods yield laminate structures<sup>25–31</sup>, surface modification of the substrate material is an attractive route to skin formation due to its simplicity, good adhesion inter-layer adhesion properties promoting resilience to delamination upon strain<sup>25,32–35</sup>.

Elastomeric polydimethylsiloxane (PDMS) has been the substrate of choice for soft lithography<sup>36</sup>, in part due to its optical transparency, nm-replication fidelity, surface adhesion and bulk mechanical properties, and ease of handling. PDMS readily undergoes surface oxidation and vitrification via plasma exposure or UV ozonolysis (UVO)<sup>37–40</sup>, yielding a high modulus ( $\sim$  GPa<sup>41</sup>) silica-like layer. While UVO exposure yields glassy skins of approximate 1-10  $\mu$ m thickness,<sup>38,42,43</sup> oxygen or air plasmas generally lead to much thinner films, of the order of a few to tens of nm.

Uniaxial bilayer compression ( $\epsilon$ ) of thin layers of PDMS results in a well-known mechanical instability<sup>44</sup> yielding sinusoidal surface patterns, in the low deformation limit, with wavelength

$$\lambda = 2\pi h \left( \frac{\bar{E}_f}{3\bar{E}_s} \right)^{\frac{1}{3}} \quad (1)$$

and amplitude

$$A = h \left( \frac{\epsilon}{\epsilon_c} - 1 \right)^{\frac{1}{2}} \quad (2)$$

where  $h$  and  $\bar{E}_f$  are, respectively, the skin thickness and plane strain modulus,  $\bar{E}_s$  is the modulus of (thick  $\gg$   $h$ ) substrate, and  $\epsilon_c$  is a critical strain<sup>45,46</sup> which must be exceeded to induce the instability. In this limit, only  $A$  depends on  $\epsilon$ , providing a powerful means to decouple  $\lambda$  from  $A$  in surface patterning. Taking typical values for the elastic modulus of PDMS  $E_{PDMS} = 1.6$  MPa, Poisson ratio  $\nu = 0.5$  (yielding  $\bar{E}_s = E/(1 - \nu^2) \simeq 2.1$  MPa), and for the glassy skin  $\bar{E}_f \simeq 1$ -30 GPa, one can expect a lower limit for  $\lambda$  to

<sup>a</sup> Department of Chemical Engineering, Imperial College London, London SW7 2AZ, UK. E-mail: j.cabral@imperial.ac.uk

† Electronic Supplementary Information (ESI) available: [details of any supplementary information available should be included here]. See DOI: 10.1039/b000000x/

‡ Dedicated to the memory of Arnaud Chiche.

be of the order of 100 nm for plasma oxidation and tens of  $\mu\text{m}$  for UVO.

Significantly, skin formation by oxidation has been found to evolve as a frontal process,<sup>47–49</sup> where the surface densification occurs alongside an increase in skin thickness. Three stages - induction, formation, and propagation - could be identified, detailed in the Supplementary Information, and sufficient modulus contrast between the skin and PDMS substrate shown to occur by the first stage. The skin thickness was found to increase logarithmically with exposure time,  $h \propto \ln(t)$ , and a change of log slope was observed after saturation (i.e. when maximum skin conversion takes place, and only the layer thickness increases).

Recalling the critical strain condition, where  $\varepsilon > \varepsilon_c$ , given by

$$\varepsilon_c = \frac{1}{4} \left( \frac{3\bar{E}_s}{\bar{E}_f} \right)^{\frac{2}{3}} \quad (3)$$

the film modulus must exceed  $\bar{E}_f > 3\bar{E}_s(4\varepsilon_c)^{-3/2}$  which corresponds to a minimum glassy thickness  $h_{min}$  set by the planar front propagation kinetics. In simple terms, reducing the skin thickness by a shorter oxidation process should no longer meet the buckling condition, at constant  $\varepsilon$ , and is thus not a viable strategy for decreasing  $\lambda$ .

We have recently examined the PDMS frontal vitrification by oxygen and air plasma exposure and experimentally attained a lowest boundary for the wavelength of  $\simeq 100$  nm at  $\varepsilon_{prestrain} \approx 20\%$ <sup>48,49</sup>. This  $\lambda_{min}$  was obtained by an optimal choice of plasma frequency, gas pressure, oxygen content, and exposure time,<sup>49</sup> already in the high deformation (sinusoidal) regime<sup>50–55</sup>. Under these conditions, the wavelength ( $\lambda_{HD}$ ) and amplitude ( $A_{HD}$ ) decrease with  $\varepsilon$  according to

$$\lambda_{HD} = \frac{\lambda}{(1+\varepsilon)(1+\xi)^{1/3}} \quad (4)$$

$$A_{HD} = \frac{A}{(1+\varepsilon)^{1/2}(1+\xi)^{1/3}} \quad (5)$$

where  $\xi = 5\varepsilon(1+\varepsilon)/32$ , with  $\lambda$  and  $A$  defined in eqs. 1 and 2., respectively.

Inspection of eqs. 1-5 suggests that, in addition to decreasing  $h$ , which is constrained by the frontal skin growth itself, increasing  $E_{PDMS}$  or decreasing  $\bar{E}_f$  would also yield a reduction in  $\lambda$  (or  $\lambda_{HD}$ ). However, the cubic root dependence of the ratio of moduli yields a weak variation of  $\lambda$  by tuning  $E_{PDMS}$  (e.g. stiffening the substrate by curing conditions or addition of reinforcing fillers). For instance, doubling the PDMS modulus decreases  $\lambda$  by only 20% but increases  $\varepsilon_c$  by 60% and, as discussed above,  $\varepsilon$  is generally limited by material failure.

This paper seeks to devise strategies to extend the pattern dimensions attainable by mechanical wrinkling of surface-oxidised PDMS to the sub-100 nm range, with application ranging from nano-patterning to optics and photonics in the visible to deep UV, without resorting to lithographic or clean-room facilities.

## 2 Experimental

### 2.1 Sample preparation

PDMS elastomers (Sylgard 184, Dow Corning) were prepared at selected base:crosslinker ratios, degassing for 15 min under vacuum, casting onto a glass plate at room temperature for 3h, and then thermally cured in a convection oven at a temperature  $T$ . Unless stated otherwise, base:crosslinker=10:1, and  $T = 75$  °C. Coupons of 1 cm  $\times$  2 cm and approximately 2 mm thickness were clamped onto a strain stage and stretched by a prestrain  $\varepsilon_{prestrain}$  prior to surface oxidation. X-ray (XRR) and neutron reflectivity (NR) samples were cast onto 3 inch diameter silicon wafers (Si-Mat, Landsberg/Lech, Germany) previously cleaned by UVO exposure, and the bottom surface of 1 cm thick samples was investigated.

### 2.2 Surface oxidation

Surface oxidation was performed by means of plasma and/or UVO exposure. A 13.6 MHz plasma chamber (Harrick PDC-002) with a gas mixer (PDC-FMG-2, Harrick Plasma) was employed, generally at a power of  $p = 7.16$  W and (air) pressure of  $P = 1$  mbar. Selected experiments were also carried out with a 40 KHz plasma (Diener FEMTO), which generally yields larger  $h$  and was thus not pursued further. A UVO chamber (PSD Pro Series NOVASCAN) with distance  $d \simeq 1$  cm between sample and UV lamp was used for the UVO oxidation.

### 2.3 Specular X-ray and neutron reflectivity

XRR measurements were carried out with a PANalytical X'Pert PRO MPD diffractometer/reflectometer equipped with a Cu W/Si parabolic mirror (2.2 kW;  $\lambda_r = 1.54\text{\AA}$ ), beam attenuator (Ni 0.125mm), parallel plate collimator (0.09°) and generator power of 40 kV and 40 mA, and reflection angles  $0.1^\circ \leq \theta \leq 0.3^\circ$ . NR experiments were performed at the Figaro reflectometer (Institut Laue Langevin, Grenoble) at two angles 0.723° and 2.723°. Reflectivity data were normalised and plotted as a function of momentum transfer  $Q = 4\pi \sin(\theta)/\lambda_r$ . The scattering length density (SLD) profiles were modelled (Abeles method implemented in Motofit<sup>56</sup> and RasCal<sup>57</sup>) to determine the thickness, roughness and composition of the glassy-layer at the PDMS surface; UVO-oxidised specimens yield  $h > 1$   $\mu\text{m}$  and thus only the glassy SLD and roughness were determined.

### 2.4 Pattern characterisation

Wrinkling morphology was evaluated by atomic force microscopy (AFM) with a Bruker Innova microscope in tapping mode at 0.2 Hz with Si tips (MPP-11100-W, Bruker), and analysed with NanoScope software, as well as reflection optical microscopy (Olympus BX41M) for  $\lambda > 1$   $\mu\text{m}$ .

## 3 Results and discussion

### 3.1 Frontal glassy skin growth

Following the procedure shown in Figure 1a, pattern  $\lambda$  can be readily tuned by the glassy skin thickness  $h$ , which can be set by plasma exposure time<sup>48,49</sup>. In order to lower  $\lambda_{min}$  and access sub-

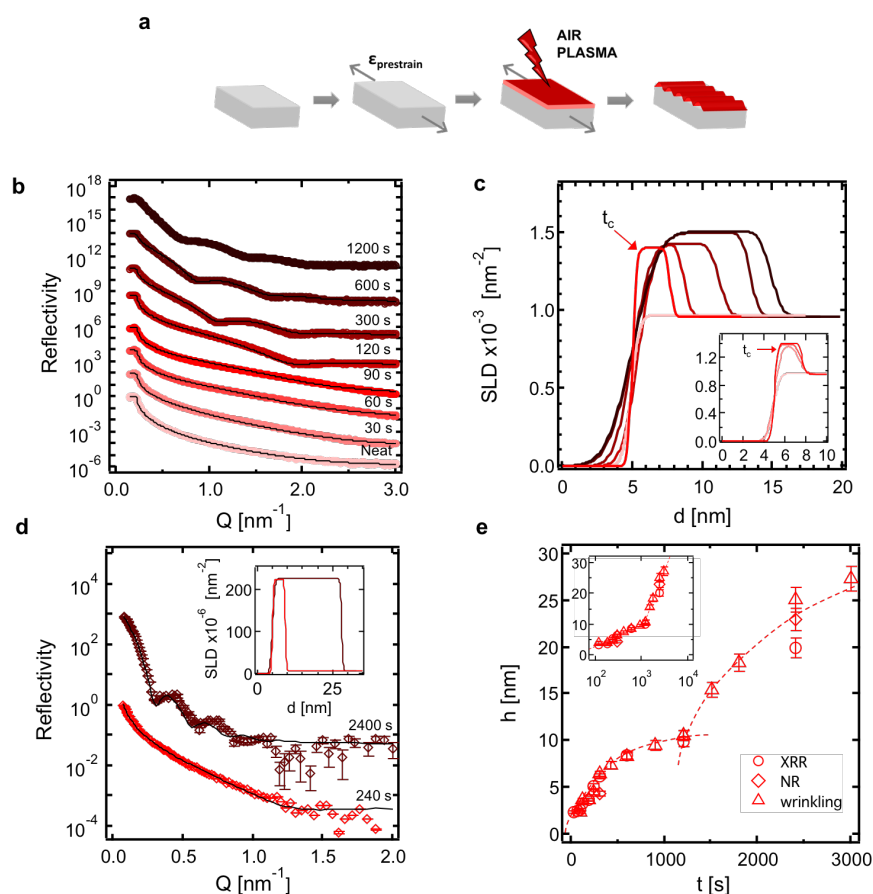


**Fig. 1** a) Schematic the glassy skin formation and mechanical wrinkling: an in-plane, uniaxial stretch ( $\epsilon_{prestrain}$ ) is applied to the PDMS coupon, which is then plasma-oxidised leading to the formation of a stiff skin (shown in red); wrinkles are formed upon compression due to strain release. b) XRR of plasma-oxidised PDMS ( $P = 1$  mbar,  $p = 7.16$  W) for different time intervals, up to 20 min, and fitted with scattering length density (SLD) profiles shown in (c). Data shifted vertically for clarity. c) Corresponding XRR SLD profiles with inset showing the initial stages of densification of the oxide layer, up to the critical time  $t_c = 90$  s when the SLD value 'saturates'. d) NR profiles and corresponding SLD shown in inset, for selected plasma exposure times. e) Oxide layer thickness as function of plasma exposure time ( $P = 1$  mbar,  $p = 7.16$  W) obtained from XRR, NR wrinkling data ( $\epsilon_{prestrain} \approx 20\%$ ) in the high deformation (HD) regime.

100 nm patterns, we first elucidate the glassy skin film formation by XRR of plasma-oxidised samples, in their relaxed state, with plasma exposure times  $t$ , from 30 to 1200 s, as shown in Figure 1b.

All data could be modeled with a single oxide layer sandwiched between air (SLD=0) and a PDMS substrate (SLD (PDMS) $_{XRR} = 9.61 \times 10^{-4} \text{ nm}^{-2}$ ,  $h \gg 1 \mu\text{m}$ ), with roughness at both interfaces, as shown in Figure 1c. The inset depicts the SLD profiles for samples exposed for times up to  $t_c = 90$  s, when the SLD of the oxide layer reaches a first plateau. This value coincides with the exposure yielding the smallest  $\lambda$  in mechanical wrinkling experiments, corroborating our interpretation that a finite thickness ( $h \approx 3$  nm) and sufficient PDMS conversion are required for the instability to be triggered (further explanation in Supplementary Information).

NR provides complementary measurements of the same laminate profiles, whose contrast now arises from the neutron SLD, as shown in Figure 1d. Data were fitted with the same model, but now with SLD(PDMS) $_{NR} = 6 \times 10^{-6} \text{ nm}^{-2}$ . Figure 1e compiles data for  $h$ , the oxide layer thicknesses, as a function of air plasma

exposure time (air,  $P = 1$  mbar,  $p = 7.16$  W) obtained from XRR, NR and wrinkling experiments (eq 4) at  $\epsilon_{prestrain} \approx 20\%$ , with values of  $\bar{E}_f$  from 3 to 6 GPa. The three independent measurements are in good agreement and establish the kinetics of the glassy skin formation. As predicted by our frontal front propagation model<sup>47</sup> (detailed in Supplementary Information), a double logarithmic kinetics is found, where  $h = a \ln(t) + b$  ( $a=495.5$ ,  $b=-463.7$  in the 'formation regime';  $a=1684.3$ ,  $b=2898.5$  in the 'propagation regime'). We find  $h_{min}$  to be 3 nm for  $\epsilon > \epsilon_c$  at 20%, corresponding to  $\bar{E}_f = 3$  GPa.

### 3.2 Plasma duration, power, pressure, gas and prestrain

We next turn to surface topography measurements by AFM. As a reference, we take the wrinkling of PDMS elastomer cured at a base:crosslinker = 10:1,  $T = 75$  °C, oxidised by air plasma ( $P = 1$  mbar,  $p = 7.16$  W,  $t = 2400$  s), uniaxially strained by  $\epsilon_{prestrain} \approx 20\%$ , shown in Figure 2a. We have previously found that plasma dose ( $D \equiv p \times t$ ) enables the collapse of all  $\lambda$  data acquired at different powers and times<sup>48</sup>, establishing  $D$  as the control variable. Further control of the skin growth kinetics, could

be achieved by systematically investigating gas composition and pressure  $P$ <sup>49</sup>.

Figure 2b compiles results for plasma-induced wrinkling  $\lambda$  as a function of  $D/P$  (air plasma), including the reference point. By decreasing  $D/P$  a *minimum* wavelength  $\lambda_{min} \approx 100$  nm could be obtained by reducing exposure time to  $t = 90$  s, for a 13.6 MHz air plasma, with a high pressure of  $P = 1.2$  mbar, and lowest induction power  $p = 7.16$  W, and  $\epsilon_{prestrain} \approx 20\%$ .

Decreasing exposure time below 90 s, in order to further decrease  $h$  and thus  $\lambda$ , yielded no wrinkling, enabling us to define a critical plasma  $t_c$  (and  $D_c$ ) that must be exceeded, at the selected strain  $\epsilon$ . Following eq. 3, we conclude that  $\bar{E}_f(t < t_c)$  yields  $\epsilon_c > 20\%$ , corresponding to the value of prestrain utilised;  $\epsilon_{prestrain}$  up to 50% at this  $t_c$  equally produced no wrinkling. Figure 2c shows the effect of increasing  $\epsilon_{prestrain}$  on  $\lambda$ , which is well described by eq. 4, as previously reported<sup>58</sup>. Depending on coupon geometry, there is an effective upper limit of approximately 65%, set by material failure and resulting in irreproducibility. The  $\lambda$  reduction with respect to reference  $\epsilon_{prestrain} = 20\%$  strain is limited to less than 15% decrease.

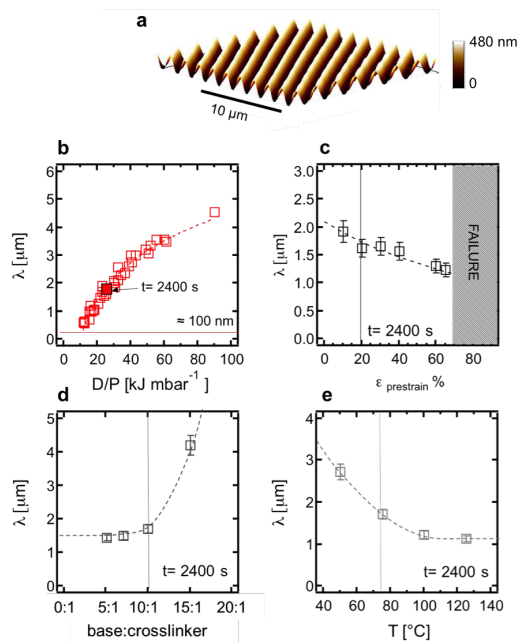


**Fig. 2** a) AFM scan of wrinkling pattern obtained by uniaxial strain relaxation with  $\epsilon_{prestrain} \approx 20\%$  of surface oxidised PDMS using reference parameters: base:elastomer ratio 10:1, curing  $T = 75$  °C, 13.6 MHz air plasma,  $t = 2400$  s,  $P = 1$  mbar, and  $p = 7.16$  W. b) Effect of plasma dose to pressure ratio ( $D/P$ ) on PDMS wrinkling wavelength  $\lambda$  with  $\epsilon_{prestrain} \approx 20\%$ , following<sup>49</sup>. c) Effect of varying  $\epsilon_{prestrain}$ , d) base:crosslinker ratio and e) curing temperature on surface  $\lambda$ , with respect to reference parameters. Line in b) is a log fit to the frontal model (Supplementary information), in c) is a fit to eq. 4, and in d) and e) are guides to the eye.

### 3.3 PDMS modification

Having shown that  $h$  and  $\bar{E}_f$  cannot be lowered further by reducing the plasma exposure time (or dose) or tuning process parameters, we consider next increasing  $\bar{E}_s$  as a strategy to reduce  $\lambda_{min}$ .

Increasing substrate stiffness can be achieved by decreasing the

base:elastomer ratio, by varying curing temperature (or time) or by addition of fillers. The resulting increase in PDMS modulus has been studied in some detail<sup>59–61</sup> and its impact on  $\lambda$  is shown in Figures 2(d) and (e). Doubling the crosslinker content only reduces  $\lambda$  by  $\approx 15\%$ , while increasing  $T$  yields a 30% decrease, keeping all other parameters constant.

The combined effects of decreasing the base:crosslinker ratio, increasing  $T$  (or time) on the resulting pattern morphology was evaluated as a function of plasma dose (Figure SI2-3). The  $\lambda$  reduction for a reference pattern of  $\approx 1$   $\mu\text{m}$  reached a maximum of 32%. However, the reduction at the smallest lengthscales are considerably smaller ( $\approx 20\%$ ). We therefore conclude that these incremental methods are not enough effective to access sub-100 nm patterning by plasma oxidation and mechanical-induced wrinkling of PDMS.

### 3.4 Double frontal UVO and air plasma oxidation approach

We now consider the possibility of coupling UVO and plasma oxidation, into a double oxidation approach. Like oxygen or air plasmas, UVO exposure of PDMS generates a glassy skin, albeit with a much larger thickness and non-uniform profile<sup>38,41</sup>, resulting from the combined UV exposure and oxygen reactivity at the surface. Employing XRR, we resolve the densification of the PDMS surface upon UVO oxidised PDMS, as shown in Figure 3, whose SLD is shown in Figure 3c. While XRR is not suitable to determining the thickness of the glassy skin, this has been previously studied<sup>38</sup> and can be estimated from wrinkling measurements. Evidently,  $h_{UVO} \gg h_{plasma}$  by comparison of Figures 1c and 3b, of the order of 1  $\mu\text{m}$ , and SLD of the surface skin increases gradually over tens of minutes of exposure.

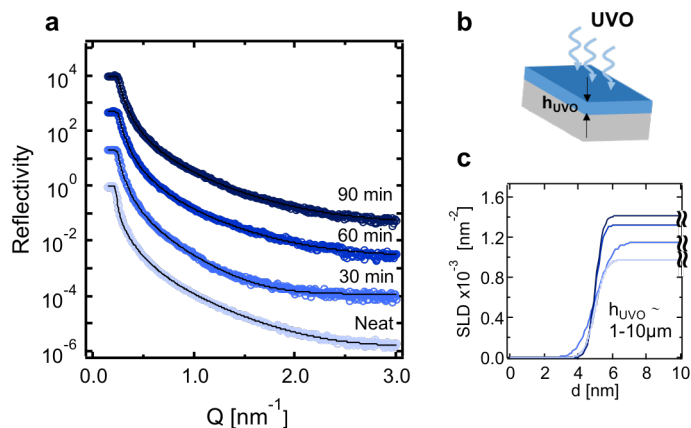


**Fig. 3** XRR measurements of PDMS specimens treated by UVO oxidation for up to 90 min exposure. (a) Normalised reflection profiles (shifted vertically for clarity) and corresponding fit (black lines). (b) Schematic of PDMS UVO oxidised, yielding a thick surface glassy skin with thickness  $h_{UVO}$ . (c) XRR SLD profiles obtained from data fits in (a).

Comparative mechanical wrinkling experiments were first performed on bilayers, prestrained by  $\epsilon_{prestrain} \approx 20\%$ , obtained by separate air plasma or UVO exposures, whose resulting  $\lambda$  are shown in Figure 4. Plasma exposure yields bilayer wrinkling with  $\lambda$  ranging between  $\approx 100$  nm and  $\approx 5$   $\mu\text{m}$ , compared to a much

greater  $\approx 20$  to  $100 \mu\text{m}$  for UVO. Despite the scale difference, the front kinetics remain qualitatively similar, with  $\lambda \propto \ln(t)$  and a 'critical time'  $t_c$  required for plasma or UVO exposure, at constant  $\epsilon_{prestrain}$ , below which the surface instability is not triggered. The value  $t_c$  in case of UVO oxidation is strain-dependent and while for  $t < t_c$ ,  $\epsilon_c > 20\%$ , increasing  $\epsilon_{prestrain}$  to 50% yields a decrease to  $t_c = 30$  min. For plasma-exposed samples, we identify as well a saturation time  $t_s$ , where the log slope changes, and which marks the transition between the 'film formation', where the film densifies and thickens, and 'film propagation' regimes, where only film propagation takes place, after full surface conversion is attained (further information in SI). Plasma exposure yields  $h_{plasma} \approx 1\text{-}30$  nm, while UVO yields a much thicker ( $h_{UVO} \approx 3 - 20 \mu\text{m}$ ) gradient, oxide layer<sup>38</sup>. In short, each vitrification process yields a glassy skin that propagates as a planar front, yielding  $h_{plasma} \ll h_{UVO}$  and  $E_{plasma}$  smaller than  $E_{UVO}$ , which albeit rises comparatively slowly upon exposure.

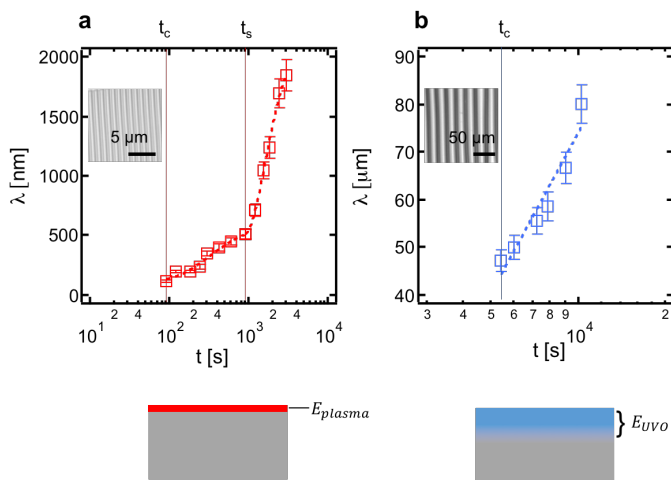


**Fig. 4** a) Sinusoidal wrinkles wavelengths for PDMS samples pre-stretched by  $\epsilon_{prestrain} \approx 20\%$  and oxidised by means of MHz plasma, as a function of exposure time. The lines correspond to logarithmic fittings. The values  $t_c$  and  $t_s$  correspond to 90 and 900 s, respectively. Induction power and air pressure were kept constant respectively at  $p = 7.16$  W and  $P = 1$  mbar. b) Wavelength of wrinkles obtained by applying mechanical strain  $\epsilon_{prestrain} \approx 20\%$  to bilayers resulting from UVO treatment of PDMS, as a function of exposure time. The line represents a logarithmic fitting. The value  $t_c$  corresponds to 90 min. Optical microscopy images of representative wrinkled samples are shown in the insets of both panels. The schematic below the panels show the impact of the two oxidative processes on bulk PDMS. Plasma oxidation results in the formation of a thinner, stiffer oxide layer compared to UVO, which leads to gradient layers<sup>38</sup>. The differences in layer elastic moduli and thicknesses justify the different pattern dimensions attainable with the two processes.

Encouraged by the  $\lambda_{min}$  reduction afforded by the increase in  $\bar{E}_s$ , we explore whether the thick oxide layer resulting from UVO treatment, can serve as a substrate and be further oxidised via plasma treatment to obtain a trilayer on which wrinkling can be induced. The process is depicted in Figure 5. XRR experiments on PDMS treated with UVO followed by air plasma oxidation confirmed the formation of two layers, with mismatching SLDs, and hence mechanical properties, as shown in Figure 6.

Since  $h_{plasma} \ll h_{UVO} \ll$  PDMS thickness, we expect wrin-

gling at each interface to be decoupled. Under these circumstances, two critical strains can be defined,  $\epsilon_{c1}$  between PDMS and the UVO skin, and  $\epsilon_{c2}$  between the upper plasma skin and UVO layer. Upon strain relaxation, we expect wrinkling from the top bilayer alone provided that  $\epsilon_{c1} < \epsilon_{prestrain} < \epsilon_{c2}$ , with

$$\epsilon_{c1} = \frac{1}{4} \left( \frac{3\bar{E}_{PDMS}}{\bar{E}_{f1}} \right)^{\frac{2}{3}} \quad (6)$$

$$\epsilon_{c2} = \frac{1}{4} \left( \frac{3\bar{E}_{f1}}{\bar{E}_{f2}} \right)^{\frac{2}{3}} \quad (7)$$

with no wrinkling arising from the intermediate UVO layer and PDMS substrate. Experiments on UVO oxidised PDMS yielded no wrinkling for  $\epsilon_{prestrain} \approx 20\%$ , and UVO exposure shorter than 90 min, indicating a value of  $\epsilon_c > 20\%$  at these conditions. Higher order patterns are obtained beyond this threshold, **when both critical strains are exceeded**, resulting from trilayer<sup>62–64</sup> wrinkling. We therefore employ a UVO treatment time of 30 and 60 min, on PDMS specimens prestrained by 20%, which are then oxidised via plasma exposure for different time intervals. Figure 7a shows wrinkling  $\lambda$  as a function of plasma treatment time, for different prior  $t_{UVO}$ . The data show that  $\lambda$  still increases logarithmically with the plasma exposure time, suggesting that the frontal vitrification model still applies<sup>47–49</sup> (refer to Supplementary Information). By UVO pretreating PDMS surfaces, the critical plasma exposure time can be lowered to  $t_c = 60$  s (from the value of 90 s in case of sole air plasma oxidation), when  $t_{UVO} = 30$  min, or  $t_c = 30$  s when  $t_{UVO} = 60$  min. This is expected given that UVO results in a partial oxidation of PDMS, prior to plasma exposure thus reducing the additional  $t_c$ . The coupling of an increase in the substrate elastic modulus ( $\bar{E}_{f1}$ ) and a decrease in the critical exposure time (leading to smaller  $h_{min}$  and  $\bar{E}_{f2,min}$  compared to the case when  $t_{UVO} = 0$ ), yielded a significant reduction in the minimum pattern wavelength attainable with this method. A  $\lambda_{min} = 45$  nm is thus readily obtained with  $t_{UVO} = 60$  min and  $t_{plasma} = 30$  s, at modest  $\epsilon_{prestrain} = 20\%$  and without PDMS modifications. Representative AFM images of wrinkled surfaces produced by  $t_{UVO} = 60$  min and various  $t_{plasma}$  are shown in Figure 7b. **Note that the order of the oxidation processes is crucial in attaining these low periodicities, and a plasma followed by UVO exposure does not yield comparable results, likely due to the glassy-skin barrier to UVO-induced layer propagation.** Modifying PDMS curing conditions as described in the previous section did not lead to a further reduction in the wavelength, as it would simply impact the wrinkling instability occurring between the bulk PDMS and UVO layer, deliberately suppressed with the prestrain chosen.

## 4 Conclusions

We have investigated the limits of plasma oxidation for bilayer formation and nanoscale wrinkling of PDMS, **and how these can be overcome by a simple, sequential UVO and plasma exposure.** A minimum wavelength of  $\lambda_{min} \approx 100$  nm was attained when plasma-oxidising PDMS samples prestrained by  $\epsilon_{prestrain} \approx 20\%$  in a single step. X-ray and neutron reflectivity experiments on oxidised PDMS provided insight into the mechanism of film for-

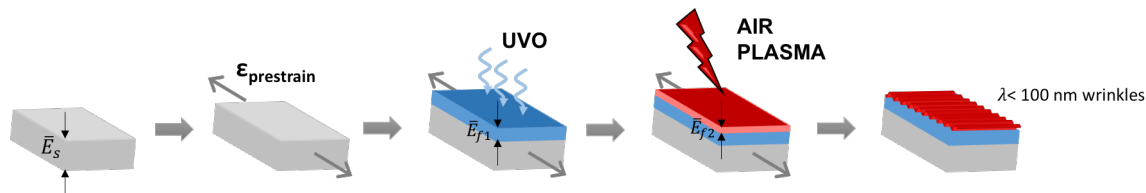


**Fig. 5** Formation of wrinkles on air plasma oxidised/UVO oxidised PDMS bilayers. A neat PDMS specimen is pre-strained uniaxially by  $\epsilon_{prestrain}$ , then exposed to UVO for  $t_{UVO}$ , leading to the formation of a layer with plane elastic modulus  $\bar{E}_{f1}$ , followed by air plasma exposure for  $t_{plasma}$  (MHz,  $p = 7.16\text{W}$ ,  $P = 1\text{mbar}$ ) resulting in the formation of a second layer with plane modulus  $\bar{E}_{f2}$ . Henceforth the strain is removed and sinusoidal wrinkling patterns with sub-100 nm  $\lambda$  are observed.

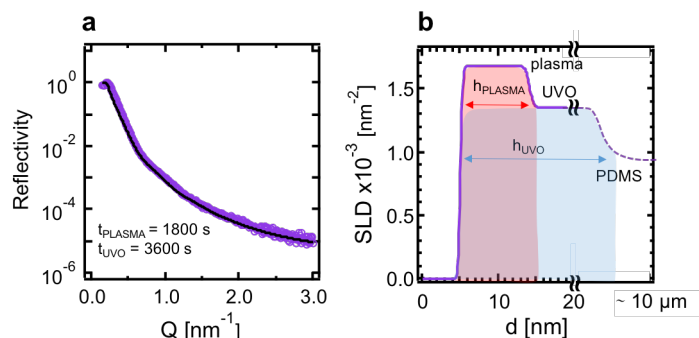


**Fig. 6** a) XRR measurements on PDMS specimens treated with subsequent UVO ( $t_{UVO} = 3600\text{ s}$ ) and air plasma oxidation ( $t_{plasma} = 1800\text{ s}$ ,  $P = 1\text{ mbar}$ ,  $p = 7.16\text{ W}$ ) according to the process in Figure 5. Normalised scattered intensity is plotted as a function of  $Q$ . Both experimental data (scatter) and the corresponding fitting (black line, resulting from the assumption of a bilayer model) using RasCal are presented. b) XRR scattering length density profiles obtained from the reflectivity curves fitting. Two distinct layers could be identified, of thicknesses  $h_{UVO}$  and  $h_{plasma}$ , resulting from the subsequent oxidative processes.

mation and densification. Analyses of scattering length density (SLD) profiles confirmed the existence of a critical exposure time  $t_c$  that must be overcome in order to yield glassy films with sufficient conversion, guaranteeing the modulus mismatch required for wrinkling (at finite  $\epsilon$ ). The findings above confirmed the impossibility of lowering the film's thickness in order to reduce  $\lambda_{min}$  attainable. Based on the wrinkling equations, we explored the impact of increasing  $\epsilon_{prestrain}$  as well as  $\bar{E}_s$  on the corresponding wrinkles obtained upon surface oxidation.  $\bar{E}_s$  was varied systematically by changing the base:crosslinker ratio, as well as the curing temperature (or time) in PDMS elastomer curing. A maximum wavelength reduction of  $\approx 30\%$  was achieved when tuning these variables.

In an attempt to further lower the pattern dimensions, and access sub-100 nm patterns, we explored the possibility of combining air plasma with ultra-violet ozonolysis (UVO) treatment. Control wrinkling experiments on UVO oxidised PDMS samples, pre-stretched by  $\epsilon_{prestrain} \approx 20\%$ , showed the existence of a critical exposure time of approximately 90 min. XRR measurements of PDMS oxidised by UVO followed by air plasma revealed the formation of two distinct layers, with mismatched SLD. Although trilayers exhibit complex wrinkling behaviour, by keeping the UVO treatment time below 90 min, we could suppress wrinkling between UVO oxide layer and the bulk PDMS, allowing only the

top, plasma oxidised film, to wrinkle. In the latter mechanism, the UVO oxidised layer acts effectively as the substrate, with an elastic modulus higher than neat PDMS. Being the substrate already oxidised to some extent, the critical time required for plasma exposure decreased thus  $\lambda_{min}$  was readily reduced to  $\approx 45\text{ nm}$  via **this double exposure method**. By changing the plasma treatment time, we observed a logarithmic increase of the wrinkling wavelength, confirming that the process proceeds with a frontal mechanism, as previously found with single plasma oxidation<sup>48,49</sup>. This simple approach considerably extends the limits of PDMS surface oxidation for nanoscale patterning, with potential applications in optics and photonics, nanofluidics, as well as template formation and contact printing.

## 5 Acknowledgements

The authors thank the Department of Chemical Engineering for a scholarship for MN, Philip Gutfreund for assistance during the experiments at ILL, and Joanne Lingling Liao for providing useful supporting data. We are grateful to Arnaud Chiche (DSM) for numerous inspiring discussions about wrinkling and soft mechanics. Data are available upon request: please contact polymer-microfluidics@imperial.ac.uk.

## References

- 1 C. D. O'Connell, M. J. Higgins, S. E. Moulton and G. G. Wallace, *J. Mater. Chem. C*, 2015, **3**, 6431–6444.
- 2 M. Kim, D.-J. Kim, D. Ha and T. Kim, *Nanoscale*, 2016, **8**, 9461–9479.
- 3 M. Altissimo, *Biomicrofluidics*, 2010, **4**, 026503 (1–6).
- 4 A. A. Tseng, K. Chen, D. C. Chii and J. M. Kung, *IEEE Trans. Electron. Packag. Manuf.*, 2003, **26**, 141–149.
- 5 H. He, J. C. She, Y. F. Huang, S. Z. Deng and N. S. Xu, *Nanoscale*, 2012, **4**, 2101–2108.
- 6 M. Moon, S. Lee, J. Sun, K. Oh, A. Vaziria and H. J.W., *Scripta Materialia*, 2007, **57**, 747–750.
- 7 L. Guo, *Adv. Mater.*, 2007, **19**, 495–513.
- 8 C. Peroz, S. Dhuey, M. Cornet, M. Vogler, D. Olynick and S. Cabrini, *Nanotechnology*, 2012, **23**, 015305.
- 9 L. J. Guo, *J. Phys. D: Appl. Phys.*, 2004, **37**, R123.
- 10 A. Pimpin and W. Srituravanich, *Eng. J.*, 2012, **16**, 37–55.
- 11 V. R. Manfrinato, L. Zhang, D. Su, H. Duan, R. G. Hobbs, E. A. Stach and K. K. Berggren, *Nano Letters*, 2013, **13**, 1555–1558.
- 12 N. Wu and R. W.B., *Nano Today*, 2009, **4**, 180–192.

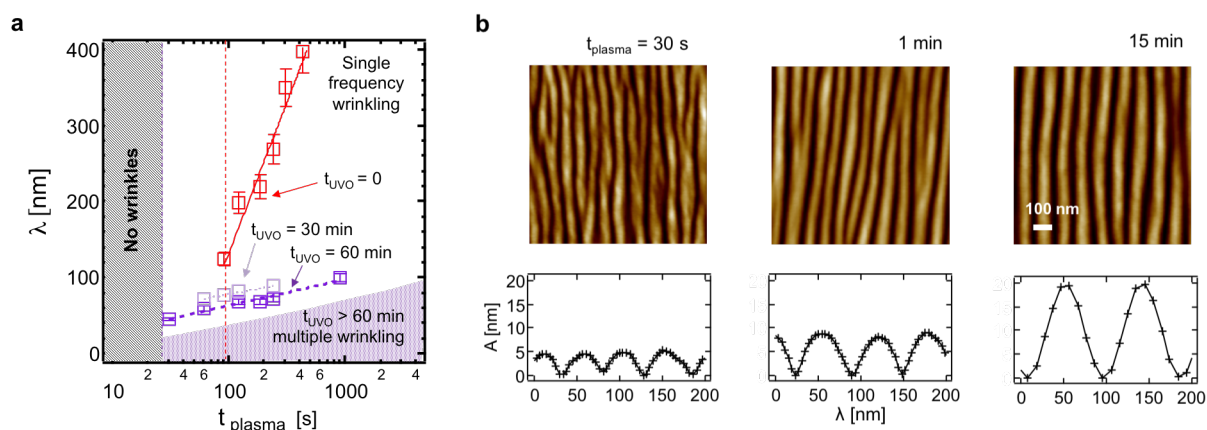


**Fig. 7** a) Wavelength of the wrinkles obtained using the procedure detailed in Figure 6, as a function of air plasma ( $p = 7.16$  W,  $P = 1$  mbar) treatment time, for species prestrained by  $\epsilon_{prestrain}$  and pre-treated via UVO exposure for 0, 30 and 60 minutes. The lines correspond to a logarithmic fitting. b) AFM tapping mode topographies of wrinkling patterns obtained by subsequent UVO ( $t_{UVO} = 60$  min) and air plasma ( $P = 1$  mbar,  $p = 7.16$  W) exposure of a PDMS specimen upon relaxation of uniaxial strain  $\epsilon_{prestrain} \approx 20\%$ .

- 13 M. J. Fasolka and A. M. Mayes, *Annu. Rev. Mater. Res.*, 2001, **31**, 323–355.
- 14 A. del Campo and E. Arzt, *Chemical Reviews*, 2008, **108**, 911–945.
- 15 J. Genzer and J. Groenewold, *Soft Matter*, 2006, **2**, 310–323.
- 16 J. Groenewold, *Phys. A*, 2001, **298**, 32–45.
- 17 B. Li, Y.-P. Cao, X.-Q. Feng and H. Gao, *Soft Matter*, 2012, **8**, 5728–5745.
- 18 J. B. Kim, P. Kim, N. C. Pegard, S. J. Oh, C. R. Kagan, J. W. Fleischer, H. A. Stone and Y.-L. Loo, *Nat. Photon.*, 2012, **6**, 327–332.
- 19 M. Li, D. Joung, B. Hughes, S. D. Waldman, J. A. Kozinski and D. K. Hwang, *Sci. Rep.*, 2016, **6**, 30463 (1–9).
- 20 E. Chan and A. Crosby, *Adv. Mater.*, 2006, **18**, 3238–3242.
- 21 V. Jokinen, M. Leinikka and S. Franssila, *Adv. Mater.*, 2009, **21**, 4835–4838.
- 22 P. Görrn, M. Lehnhardt, W. Kowalsky, T. Riedl and S. Wagner, *Adv. Mater.*, 2011, **23**, 869–872.
- 23 K. Efimenko, M. Rackaitis, E. Manias, A. Vaziri, L. Mahadevan and J. Genzer, *Nat. Mater.*, 2005, **4**, 293–297.
- 24 X. Jiang, S. Takayama, X. Qian, E. Ostuni, H. Wu, N. Bowden, P. LeDuc, D. Ingber and G. Whitesides, *Langmuir*, 2002, **18**, 3273–3280.
- 25 N. Bowden, S. Brittain, A. G. Evans, J. W. Hutchinson and G. M. Whitesides, *Nature*, 1998, **393**, 146–149.
- 26 M. Watanabe, *Polym. Adv. Technol.*, 2005, **16**, 744–748.
- 27 J. Serrano, Q. Xu and C. D.G., *J. Vac. Sci. Technol., A*, 2006, **24**, 324–327.
- 28 M. D. Casper, A. O. Gozen, M. D. Dickey, J. Genzer and J.-P. Maria, *Soft Matter*, 2013, **9**, 7797–7803.
- 29 C. M. Stafford, K. Harrison, C. and Beers, E. J. Karim, A. and Amis, M. R. VanLandingham, W. M. R. Kim, H. and Volksen and E. E. Simonyi, *Nat. Mater.*, 2004, **3**, 545–550.
- 30 Z. Chen, W. Ren, L. Gao, B. Liu, S. Pei and H.-M. Cheng, *Nat. Mater.*, 2011, **10**, 424–428.
- 31 S. J. Chae, F. Güneş, K. K. Kim, E. S. Kim, G. H. Han, S. M. Kim, H.-J. Shin, S.-M. Yoon, J.-Y. Choi, M. H. Park, C. W. Yang, D. Pribat and Y. H. Lee, *Adv. Mater.*, 2009, **21**, 2328–2333.
- 32 A. Chiche, C. Stafford and J. Cabral, *Soft Matter*, 2008, **4**, 2360–2364.
- 33 M. Pretzl, A. Schweikart, C. Hanske, A. Chiche, U. Zettl, A. Horn, A. Böker and A. Fery, *Langmuir*, 2008, **24**, 12748–12753.
- 34 N. Bowden, W. T. S. Huck, K. E. Paul and G. M. Whitesides, *Appl. Phys. Lett.*, 1999, **75**, 2557.
- 35 D. B. H. Chua, H. T. Ng and S. Li, *Appl. Phys. Lett.*, 2000, **76**, 721–723.
- 36 Y. Xia, and G. M. Whitesides, *Annu. Rev. Mater. Sci.*, 1998, **28**, 153–184.
- 37 M. M. Demir, Y. Z. Menciloglu and B. Erman, *Polymer*, 2005, **46**, 4127–4134.
- 38 K. Efimenko, W. E. Wallace and J. Genzer, *J. Colloid Interface Sci.*, 2002, **254**, 306–315.
- 39 M. J. Owen and P. J. Smith, *J. Adhes. Sci. Technol.*, 1994, **8**, 1063–1075.
- 40 H. Hillborg, J. Ankner, U. Gedde, G. Smith, H. Yasuda and K. Wikström, *Polymer*, 2000, **41**, 6851–6863.
- 41 S. Béfhahy, P. Lipnik, T. Pardoën, C. Nascimento, B. Patris, P. Bertrand and S. Yunus, *Langmuir*, 2010, **26**, 3372–3375.
- 42 M. Ouyang, C. Yuan, R. Muisener, A. Boulares and J. Koberstein, *Chem. Mater.*, 2000, **12**, 1591–1596.
- 43 J.-Y. Park, H. Y. Chae, C.-H. Chung, S. J. Sim, J. Park, H. H. Lee and P. J. Yoo, *Soft Matter*, 2010, **6**, 677–684.
- 44 H. Allen, *Analysis and Design of Structural Sandwich Panels*, Pergamon, 1969.
- 45 A. Volynskii, S. Bazhenov, O. Lebedeva and N. Bakeev, *J. Mater. Sci.*, 2000, **35**, 547–554.
- 46 R. Huang, *J. Mech. Phys. Solids*, 2005, **53**, 63–89.
- 47 J. T. Cabral, S. D. Hudson, C. Harrison and J. F. Douglas, *Langmuir*, 2004, **20**, 10020–10029.

- 48 F. A. Bayley, J. L. Liao, P. N. Stavrinou, A. Chiche and J. T. Cabral, *Soft Matter*, 2014, **10**, 1155–1166.
- 49 M. Nania, O. K. Matar and J. T. Cabral, *Soft Matter*, 2015, **11**, 3067–3075.
- 50 S. Cai, D. Breid, A. Crosby, Z. Suo and J. Hutchinson, *J. Mech. Phys. Solids*, 2011, **59**, 1094 – 1114.
- 51 H. Jiang, D.-Y. Khang, J. Song, Y. Sun, Y. Huang and J. A. Rogers, *Proc. Natl. Acad. Sci.*, 2007, **104**, 15607–15612.
- 52 J. Song, H. Jiang, Z. Liu, D. Khang, Y. Huang, J. Rogers, C. Lu and C. Koh, *Int. J. Solids Struct.*, 2008, **45**, 3107 – 3121.
- 53 C. Harrison, C. Stafford, W. Zhang and A. Karim, *Appl. Phys. Lett.*, 2004, **85**, 4016–4018.
- 54 H. Jiang, D.-Y. Khang, H. Fei, H. Kim, Y. Huang, J. Xiao and J. A. Rogers, *J. Mech. Phys. Solids*, 2008, **56**, 2585 – 2598.
- 55 H. Vandeparre, M. Piñeirua, F. Brau, B. Roman, J. Bico, C. Gay, W. Bao, C. N. Lau, P. M. Reis and P. Damman, *Phys. Rev. Lett.*, 2011, **106**, 224301.
- 56 A. Nelson, *J. Appl. Crystallogr.*, 2006, **39**, 273–276.
- 57 <https://sourceforge.net/projects/rscl/>.
- 58 H. Jiang, D.-Y. Khang, J. Song, Y. Sun, Y. Huang and J. A. Rogers, *Proc. Natl. Acad. Sci.*, 2007, **104**, 15607–15612.
- 59 F. Carrillo, S. Gupta, M. Balooch, S. J. Marshall, G. W. Marshall, L. Pruitt and C. M. Puttlitz, *J. Mater. Res.*, 2011, **20**, 2820–2830.
- 60 Z. Wang, A. A. Volinsky and N. D. Gallant, *J. Appl. Polym. Sci.*, 2014, **131**, 41050 (1–4).
- 61 I. Johnston, D. McCluskey, C. Tan and M. Tracey, *Journal of Micromechanics and Microengineering*, 2014, **24**, 035017(7pp).
- 62 A. Nolte, R. Cohen and M. F. Rubner, *Macromolecules*, 2006, **39**, 4841–4847.
- 63 E. Lejeune, A. Javili, J. Weickenmeier, E. Kuhl and C. Linder, *Soft Matter*, 2016, **12**, 5613–5620.
- 64 F.P.Beer, J. E. Russell Johnston, J. T. Dewolf and D. F. Mazurek, *Mechanics of materials*, McGraw Hill, New York, USA, 2012.